Multiphase Stirling Engines

Artin Der Minassians[1]
e-mail: artin.der.minassians@gmail.com

Seth R. Sanders
Professor
e-mail: sanders@eecs.berkeley.edu

Department of Electrical Engineering and
Computer Sciences,
University of California, Berkeley,
518 Cory Hall,
Berkeley, CA 94720

Analysis, design, fabrication, and experimental assessment of a symmetric three-phase free-piston Stirling engine system is discussed in this paper. The system is designed to operate with moderate-temperature heat input that is consistent with solar-thermal collectors. Diaphragm pistons and nylon flexures are considered for this prototype to eliminate surface friction and to provide appropriate seals. In addition, low loss diaphragm pistons, etched and woven-wire screen heat exchangers, and plastic flexures, as the main components of the system, are outlined. The experimental results are presented and compared with design analysis. Experiments successfully confirm the design models for heat exchanger flow friction losses and gas spring hysteresis dissipation. Furthermore, it is revealed that gas spring hysteresis loss is an important dissipation phenomenon for low-power Stirling engines and should be carefully addressed in design. Analysis shows that the gas hysteresis dissipation is reduced drastically by increasing the number of phases in a multiphase Stirling engine system. It is further shown that for an even number of phases, half of the engine chambers could be eliminated by utilizing a reversing mechanism within the multiphase system. The mathematical formulation and modal analysis of multiphase Stirling engine system are then extended to a system that incorporates a reverser. By introducing a reverser to the fabricated prototype, the system successfully operates in engine mode. The system proves its self-starting capability and validates the computed start-up temperature. [DOI: 10.1115/1.3097274]

1 Introduction

In its various forms, renewable energy is derived directly from the sun, or from heat generated deep within the earth. Examples of renewable energy are electricity and heat generated from solar, wind, ocean, hydropower, biomass, geothermal resources, biofuels, and hydrogen derived from renewable resources. It is astonishing when we realize that the earth receives more energy from the sun in just one hour than the world population uses in a whole year. Current solar technologies include conventional photovoltaics (PV), thin-film PV, concentrated PV, solar power tower, solar parabolic trough, solar dish-engine, and residential water heating. The main challenge in all the above-mentioned technologies is to reduce the cost of the generated electricity and to make it competitive with the cost of the electricity that is derived from fossil resources.

A low-cost solar-thermal-electric technology has been outlined by the authors [1,2]. The proposed energy conversion system is conceived to convert solar power into electricity in three stages: solar power to heat, heat to mechanical power, and mechanical power to electricity. Low-concentration nonimaging solar collectors are capable of delivering thermal power at temperatures in the range of $180-250\,^{\circ}\mathrm{C}$ without having to track the sun [3]. A nontracking system avoids the costs and maintenance issues associated with tracking collectors with high concentration ratios. Thus, a nonimaging solar collector is a very suitable component to serve as the first energy conversion stage of the proposed system.

A Stirling engine, in the proposed system, is utilized to convert the delivered heat by the solar concentrator into mechanical power. One potential advantage of the Stirling cycle is the possibility of using air as the working fluid, and thus avoiding issues with long-term containment and the associated maintenance requirements. Furthermore, recent success in demonstrating very low differential temperature engines is also compelling [4]. In the system conceived here, the Stirling engine converts moderate-temperature heat to electricity by way of integrated electric gen-

eration. However, the use of low-temperature heat limits the theoretical maximum thermodynamic efficiency achievable by the heat engine, which limits the overall system efficiency to the range of 12–15% [2]. This disadvantage, however, can be compensated by lower costs in materials and in reduced maintenance. We take the view that cost effectiveness of solar electric technologies should be judged by output power per dollar rather than by efficiency or other merits [1,2].

Single-phase gamma-type Stirling engines require two pistons, namely, the displacer piston and the power piston, for successful operation. The displacer piston shuttles the working fluid back and forth between hot and cold sections of the engine, and, hence, generates an oscillatory pressure waveform inside the engine chamber. Coupling to the pressure waveform, the power piston moves and extracts the mechanical work that is produced by the Stirling thermodynamic cycle. Except for free-piston engines [5,6], displacer and power pistons are mechanically linked to provide an appropriate phase delay, which facilitates power extraction.

In a multiphase Stirling engine, each engine is an alpha-type Stirling engine that is connected to its neighboring two engines via its two pistons. A multiphase Stirling engine system must incorporate at least three engines and, hence, three pistons. There need not be mechanical linkage among pistons, as multiphase Stirling engines can be implemented as free-piston engines. The working fluid in each engine is contained within its chamber and is not exchanged nor shared with other phases. Each piston is linked to its neighboring two pistons via the pressure waveform inside corresponding engine chambers. A multiphase Stirling engine system is a good alternative to its single-phase counterparts in the following ways.

- It successfully eliminates the displacer piston and corresponding design and control problems.
- Each piston is double-acting, that is, it acts as the compression piston for one engine and as the expansion piston for the neighboring engine.
- There is only one piston per phase, which means that the system complexity is reduced relative to the displacer-type engines.
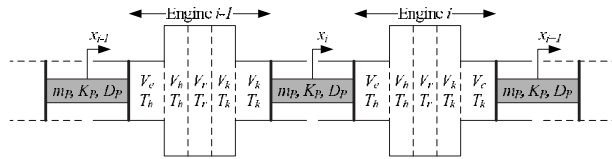- It can be self-starting.

Fig. 1 Schematic of a multiphase Stirling engine system

The general formulation of a multiphase Stirling engine is presented in this paper followed by the modal analysis of the symmetric three-phase example system. The design, fabrication, and experimental evaluation of a symmetric three-phase Stirling engine system are discussed next. The operation of the fabricated system in engine mode is evaluated and compared with the modal analysis results. An assessment of gas spring hysteresis dissipation shows that this loss effect dominates operation for the low-power three-phase machine. This leads to discussions on the theoretic formulation, modal analysis, and experimental implementation of a "reverser" mechanism in multiphase Stirling systems as a means of reducing the gas spring hysteresis dissipation of the system.

2 Formulation

Figure 1 shows the schematic of a multiphase Stirling engine. An isothermal model [5] is the simplest formulation for thermodynamic behavior of a Stirling engine, and is used in this paper to understand the qualitative system behavior. For the ith Stirling engine that operates within an N-phase system (Fig. 1), the pressure of the working fluid, p_i, is given by

$$p_i = (MR)/\left(\frac{V_{e,i}}{T_h} + \frac{V_{c,i}}{T_k} + \frac{V_k}{T_k} + \frac{V_r}{T_r} + \frac{V_h}{T_h}\right), \quad i = 1, \ldots, N \quad (1)$$

where M is the mass of the working fluid, R is the ideal gas constant, $V_{e,i}$ and $V_{c,i}$ are, respectively, the volumes of expansion and compression spaces, T_h and T_k are, respectively, the temperatures of the heater and cooler in each Stirling engine, and finally V_h, V_r, and V_k are the free volumes of the heater, regenerator, and cooler, respectively. The isothermal model presumes that the temperatures of expansion and compression spaces are T_h and T_k, respectively.

The regenerator is sandwiched between heater and cooler and is considered to be adiabatic. Assuming a linear temperature profile across the regenerator, its mean effective temperature, T_r, can then be expressed as [5]

$$T_r = \frac{T_h - T_k}{\ln(T_h/T_k)} \quad (2)$$

Furthermore, $V_{e,i}$ and $V_{c,i}$ are calculated as a function of nominal volumes of expansion and compression spaces, V_e^{nom} and V_c^{nom}, respectively, as

$$V_{e,i} = V_e^{\text{nom}} - A_P x_i \quad (3)$$

$$V_{c,i} = V_c^{\text{nom}} + A_P x_{i+1} \quad (4)$$

where x_i is the displacement of the ith piston, and A_P is the cross-sectional area of each piston.

Consider each piston to be a mass-spring subsystem (m_P, K_P), with dissipation or loading function, $f_P(\dot{x}_i)$. Each piston is coupled to its two adjacent neighbors through the working gas modeled by Eq. (1). The system of differential equations in Eq. (5), representing Newton's second law, defines the nonlinear dynamical behavior of the ith piston in a multiphase system.

$$A_P(p_{i-1} - p_i) - f_P(\dot{x}_i) - K_P x_i = m_P \ddot{x}_i \quad (5)$$

where $i = 1, \ldots, N$ and $f_P(\dot{x})$ may include any possible dissipation or loading model [2]. Note that the Nth engine is followed by the first engine in a multiphase system loop.

The simulation result of a symmetric three-phase Stirling engine system is depicted in Fig. 2. In steady state operation, the pistons have a symmetrically skewed-phase oscillatory motion, as shown in Fig. 2(b). Of course, the output power of each engine, and hence the entire system, is a function of the phase delay between volume variation in compression and expansion spaces [5].

3 Linearization

System linearization at the system equilibrium is an effective tool for qualitative analysis of nonlinear system behavior. The origin, x_0, is the equilibrium of the multiphase Stirling engine system defined by differential equations in Eq. (5). The qualitative properties of nonlinear systems in the vicinity of isolated equilibria are determined by linearization of the nonlinear system if the linearization has no eigenvalues on the $J\omega$-axis [7]. Furthermore, if the linearization has at least one eigenvalue in the open right half of the complex plane, then the origin is an unstable equilibrium for the nonlinear system [7].

Appropriate substitutions from Eqs. (3) and (4) and linearization of Eq. (5) lead to Eq. (6), which models the linearized dynamical behavior of the ith piston
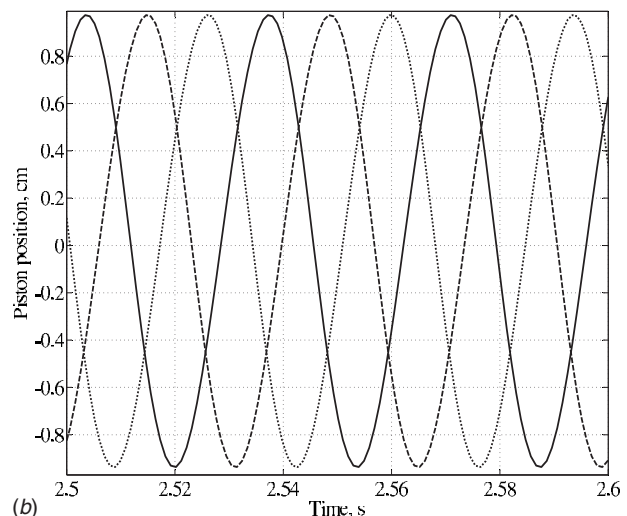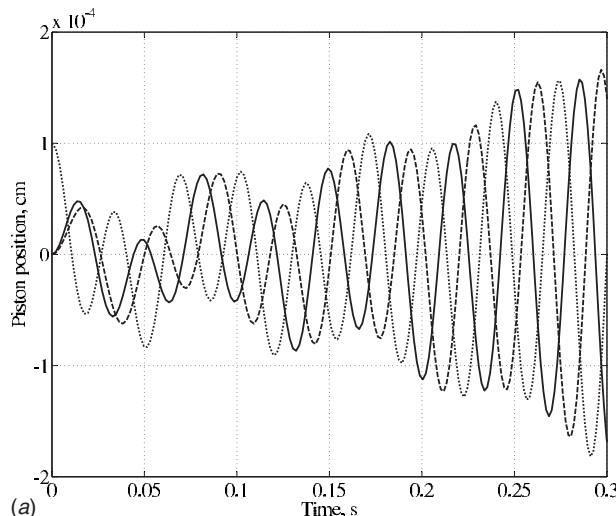

Fig. 2 Simulated piston positions of a symmetric three-phase Stirling engine system: (a) startup and (b) steady state
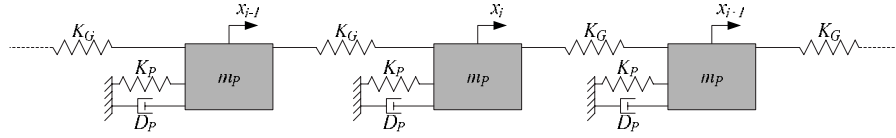
Fig. 3 Mass-spring equivalent of the multiphase Stirling engine system in Fig. 1. K_G represents the gas spring stiffness.

$$\ddot{x}_i = \left(\frac{\alpha}{m_P}\frac{1}{T_h}\right)x_{i-1} - \left(\frac{\alpha}{m_P}\frac{1}{T_h} + \frac{\alpha}{m_P}\frac{1}{T_k} + \frac{K_P}{m_P}\right)x_i + \left(\frac{\alpha}{m_P}\frac{1}{T_k}\right)x_{i+1} - d\dot{x}_i$$

$$(6)$$

where $i = 1, \ldots, N$ and

$$\alpha = (MR) \Big/ \left(\frac{V_c^{\text{nom}}}{T_k} + \frac{V_k}{T_k} + \frac{V_r}{T_r} + \frac{V_h}{T_h} + \frac{V_e^{\text{nom}}}{T_h}\right)^2 A_P^2$$

$$(7)$$

$$d = \frac{1}{m_P} \left.\frac{\partial f_P(\dot{x}_i)}{\partial \dot{x}_i}\right|_{\dot{x}_i=0}$$

Therefore, the linearization of multiphase Stirling engine system with fixed heater and cooler temperatures would be represented as a time-invariant autonomous linear system, as in Eq. (8).

$$
\begin{bmatrix} \ddot{x}_1 \\ \ddot{x}_2 \\ \ddot{x}_3 \\ \vdots \\ \ddot{x}_{N-2} \\ \ddot{x}_{N-1} \\ \ddot{x}_N \end{bmatrix} + d\begin{bmatrix} \dot{x}_1 \\ \dot{x}_2 \\ \dot{x}_3 \\ \vdots \\ \dot{x}_{N-2} \\ \dot{x}_{N-1} \\ \dot{x}_N \end{bmatrix} + \begin{bmatrix} a & -b & 0 & \cdots & 0 & 0 & -c \\ -c & a & -b & \cdots & 0 & 0 & 0 \\ 0 & -c & a & \cdots & 0 & 0 & 0 \\ \vdots & \vdots & \vdots & \ddots & \vdots & \vdots & \vdots \\ 0 & 0 & 0 & \cdots & a & -b & 0 \\ 0 & 0 & 0 & \cdots & -c & a & -b \\ -b & 0 & 0 & \cdots & 0 & -c & a \end{bmatrix}\begin{bmatrix} x_1 \\ x_2 \\ x_3 \\ \vdots \\ x_{N-2} \\ x_{N-1} \\ x_N \end{bmatrix}
$$
$$= 0 \qquad (8)$$

where

$$a = \frac{K_P}{m_P} + \frac{\alpha}{m_P}\frac{1}{T_k} + \frac{\alpha}{m_P}\frac{1}{T_h} = \frac{K_P}{m_P} + (b+c) \qquad (9)$$

$$b = \frac{\alpha}{m_P}\frac{1}{T_k} \qquad (10)$$

$$c = \frac{\alpha}{m_P}\frac{1}{T_h} \qquad (11)$$

4 Analysis

Based on the above discussion on mathematical modeling, the modal analysis of the linearized multiphase Stirling engine system will be discussed in this section. Specifically, the symmetrical three-phase system will be considered and analyzed.

Eigenvalues of the linearized multiphase system are functions of engine geometry, piston dynamical parameters, mean engine working pressure, and the heater and cooler temperatures. However, for a fabricated engine, the temperatures are the only parameters that may vary and affect the eigenvalues. Therefore, assuming that the cooler temperature remains unchanged, effect of the heater temperature, T_h, will be considered and discussed.

For the symmetric three-phase system, Eq. (8) is rewritten as

$$
\begin{bmatrix} \ddot{x}_1 \\ \ddot{x}_2 \\ \ddot{x}_3 \end{bmatrix} + d\begin{bmatrix} \dot{x}_1 \\ \dot{x}_2 \\ \dot{x}_3 \end{bmatrix} + \begin{bmatrix} \dfrac{K_P}{m_P}+(b+c) & -b & -c \\[2mm] -c & \dfrac{K_P}{m_P}+(b+c) & -b \\[2mm] -b & -c & \dfrac{K_P}{m_P}+(b+c) \end{bmatrix}
$$
$$\times \begin{bmatrix} x_1 \\ x_2 \\ x_3 \end{bmatrix} = 0 \qquad (12)$$

or simply

$$\ddot{x} + d\dot{x} + \mathbf{K}x = 0 \qquad (13)$$

where d is defined in Eq. (7). Figure 3 illustrates the mass-spring equivalent of the multiphase Stirling engine system shown in Fig. 1.

Clark's [8] linear transformation $\mathbf{x} = \mathbf{T}\mathbf{z}$ with

$$\mathbf{T} = \begin{bmatrix} \cos(0) & \sin(0) & \cos(0) \\[1mm] \cos(0) & \sin\left(\dfrac{2\pi}{3}\right) & \cos\left(\dfrac{2\pi}{3}\right) \\[2mm] \cos(0) & \sin\left(\dfrac{4\pi}{3}\right) & \cos\left(\dfrac{4\pi}{3}\right) \end{bmatrix} = \begin{bmatrix} 1 & 0 & 1 \\ 1 & \sqrt{3}/2 & -1/2 \\ 1 & -\sqrt{3}/2 & -1/2 \end{bmatrix}$$

$$(14)$$

elegantly decouples the system dynamical modes and readily exhibits its eigenvalues by converting Eq. (12) into

$$
\begin{bmatrix} \ddot{z}_1 \\ \ddot{z}_2 \\ \ddot{z}_3 \end{bmatrix} + d\begin{bmatrix} \dot{z}_1 \\ \dot{z}_2 \\ \dot{z}_3 \end{bmatrix} + \begin{bmatrix} \dfrac{K_P}{m_P} & 0 & 0 \\[2mm] 0 & \dfrac{K_P}{m_P}+\dfrac{3}{2}(b+c) & -\dfrac{\sqrt{3}}{2}(b-c) \\[2mm] 0 & \dfrac{\sqrt{3}}{2}(b-c) & \dfrac{K_P}{m_P}+\dfrac{3}{2}(b+c) \end{bmatrix}\begin{bmatrix} z_1 \\ z_2 \\ z_3 \end{bmatrix} = 0
$$

$$(15)$$

or

$$\ddot{z} + d\dot{z} + \tilde{\mathbf{K}}z = 0 \qquad (16)$$

where $\tilde{\mathbf{K}} = \mathbf{T}^{-1}\mathbf{K}\mathbf{T}$, and hence $\tilde{\mathbf{K}}$ shares the same eigenstructure with matrix $\mathbf{K}$.

For the sake of simplicity, the analysis is begun assuming $d = 0$. The effect of linear damping will be considered later on, after establishing the basis of the modal analysis. Based on this assumption, Eq. (13) becomes the classic state-space representation of a resonator, i.e., $\ddot{x} + \mathbf{K}x = 0$. The eigenvalues of such a resonator are the roots of the eigenvalues of the matrix $-\mathbf{K}$, and hence the roots of the eigenvalues of $-\tilde{\mathbf{K}}$. Therefore, if μ_1 is an eigenvalue of matrix $\tilde{\mathbf{K}}$, then λ_1 and λ_1' are two eigenvalues of the system associated with μ_1 and we have

$$\lambda_1 = \sqrt{-\mu_1} = \sqrt{|\mu_1|}e^{J((\pi/2)+(1/2)\angle\mu_1)} \qquad (17)$$

$$\lambda_1' = \sqrt{-\mu_1} = \sqrt{|\mu_1|}e^{J((3\pi/2)+(1/2)\angle\mu_1)} \qquad (18)$$

where $|\cdot|$ and $\angle$. denote the magnitude and angle of a complex number, respectively.

Matrix $\widetilde{\mathbf{K}}$ has one real and one pair of complex-conjugate eigenvalues. The real eigenvalue generates two eigenvalues for the system in Eq. (12) that are fixed on the $J\omega$-axis, and they correspond to a decoupled "zero-sequence" or simple oscillation mode, where none of the working gas volumes undergo any expansion or compression. Rather, each of the gas volumes is simply shuttled back and forth (in phase) through its respective heater, cooler, and regenerator. Hence, the frequency of this mode is independent of the gas spring stiffness and is set only by the stiffness of the piston linkage, K_P. Although this mode is of no interest from a thermodynamic point of view, it is useful in allowing an independent assessment of fluid flow losses [2,9]. The complex-conjugate eigenvalues of matrix $\widetilde{\mathbf{K}}$ are

$$\mu_1 = \left(\frac{K_P}{m_P} + \frac{3}{2}(b+c)\right) + J\frac{\sqrt{3}}{2}(b-c) \qquad (19)$$

$$\mu_2 = \left(\frac{K_P}{m_P} + \frac{3}{2}(b+c)\right) - J\frac{\sqrt{3}}{2}(b-c) \qquad (20)$$

At thermal equilibrium (i.e., $T_h = T_k$), b and c are equal. Hence

$$\mu_1 = \mu_2 = \frac{K_P}{m_P} + 3b = \frac{K_P + 3K_G}{m_P} \qquad (21)$$

$$\lambda_1 = \lambda_2 = -\lambda_1' = -\lambda_2' = J\sqrt{\frac{K_P + 3K_G}{m_P}} \qquad (22)$$

where $K_G = \bar{p}A_P^2/V_{\text{total}}$ is the isothermal gas spring stiffness, $\bar{p}$ is the mean pressure, and V_{total} is the total volume of each engine chamber [2].

The slightest temperature difference between compression and expansion spaces (i.e., $T_h > T_k$) forces μ_1 and μ_2 away from the real axis. Consequently, the two eigenvalues λ_1' and λ_2, which correspond to the "forward" three-phase operating mode [2], migrate to the right half of the complex plane, and the equilibrium becomes unstable. Therefore, the main nonlinear system becomes unstable, according to the Hartman–Grobman theorem and the indirect Lyapunov method [7]. The unstable mode is expected to grow spontaneously until a loading mechanism (e.g., the generator and electric loading) absorbs mechanical power at the same rate that it is produced. This is the intended mode of operation and makes the system become "self-starting." Note that the real part of μ, $\Re(\mu)$, is a linear function of the average value of the compression and expansion temperatures, and the imaginary part of μ, $\Im(\mu)$, is proportional to the difference of those two temperatures. Thus, it is this temperature difference that enables operation, as expected.

Also of interest is the complex pair of eigenvalues in the left half plane, λ_1 and λ_2'. This pair corresponds to "backward" three-phase operation, where mechanical power needs to be supplied at this resonant frequency to support the motion. This mode corresponds to operation as a Stirling heat pump.

The next step is to consider the effect of the system internal losses (e.g., flow friction through heat exchangers, gas spring hysteresis loss, etc.) that are represented by a linear damping factor, d. Since internal dissipation reduces the useful output work of the Stirling cycle, the system should be designed for minimal losses. For small levels of damping, the damping factor, d, approximately shifts all six λ eigenvalues (i.e., the roots of the eigenvalues of $-\mathbf{K}$) to the left by $d/2$, as depicted in Fig. 4. It moves the imaginary parts of the eigenvalues toward the center as well. However, since the latter is a small effect, it is ignored in this analysis. In the case of a nonzero damping factor, as one can observe in Fig. 4, a minimum temperature difference is required to force eigenvalues
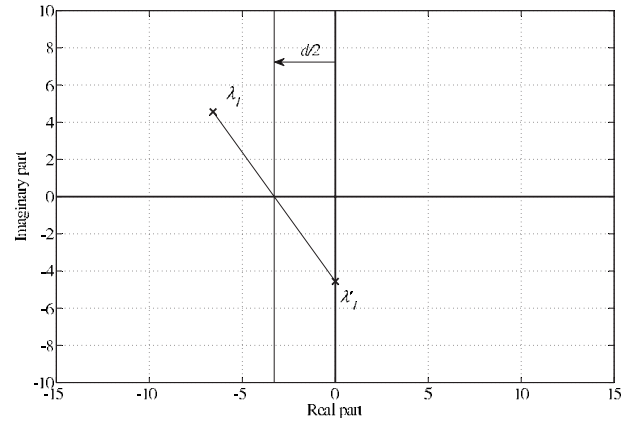

Fig. 4 Approximated effect of system dissipation on the eigenvalues

of the system to the unstable region and generate an unstable equilibrium. It is desired to estimate the minimum "start-up" temperature.

If the compression space temperature, T_k, remains unchanged, as the expansion space temperature, T_h, increases from the thermal equilibrium, the eigenvalues associated with the forward mode migrate toward the $J\omega$-axis almost in parallel to the real axis. This reasoning is based on the argument that the temperature increase does not change the gas spring stiffness significantly. Therefore, the imaginary part of the eigenvalues, which is calculated in Eq. (22), remains constant. The equilibrium becomes unstable when the eigenvalues hit the $J\omega$-axis. In this case, by utilizing trigonometric principles and identities for Fig. 4, we have

$$d = 2\Re(\lambda_1') = 2|\lambda_1'|\cos\left(\frac{3\pi}{2} + \frac{\theta}{2}\right) \qquad (23)$$

$$\sqrt{\frac{K_P + 3K_G}{m_P}} \approx -\Im(\lambda_1') = -|\lambda_1'|\sin\left(\frac{3\pi}{2} + \frac{\theta}{2}\right) \qquad (24)$$

where $\theta = \angle\mu_1$. By multiplying both sides of Eqs. (23) and (24), we have

$$d\sqrt{\frac{K_P + 3K_G}{m_P}} = -|\lambda_1'|^2\sin(3\pi + \theta)$$

$$= |\mu_1|\sin(\theta) = \Im(\mu_1) = \frac{\sqrt{3}}{2}(b-c) \qquad (25)$$

and appropriate substitutions from Eqs. (10) and (11) lead to

$$\frac{1}{T_h} = \frac{1}{T_k} - \frac{d}{\alpha}\sqrt{\frac{4}{3}m_P(K_P + 3K_G)} \qquad (26)$$

Equation (26) specifies an interesting relationship between parameters d and T_h. Given the design parameters of the engine (i.e., volumes, cold side temperature, mean working gas pressure, piston linkage mass and stiffness, and piston area), one can calculate the maximum damping factor d that will allow the symmetric three-phase Stirling engine system to start at a given T_h. Conversely, for a given damping factor d, the minimum temperature T_h that starts the engine can be calculated.

Sections 5 and 6 will discuss the fabrication and experimental assessment of a symmetric three-phase Stirling engine example that is fabricated to validate the foregoing theoretical discussion.

5 Symmetric Three-Phase Stirling Prototype

The design, fabrication, and testing of a symmetric three-phase Stirling engine system is presented in this section. The thermodynamic design parameters of the fabricated three-phase Stirling en-

Table 1 Prototype three-phase Stirling engine parameters. Volume multipliers indicate the porosity of each section.

Fluid	Ambient pressure air
MR	0.119 J/K (at 1 bar and T_k)
T_k	27°C
T_h	147°C
V_h, V_k	82.4 cm$^3 \times$ 64%
V_r	108.9 cm$^3 \times$ 53%
V_e^{nom}, V_c^{nom}	93.2 cm$^3 \times$ 100%
x_m^{nom}	1 cm
A_P	45.6 cm^2
m_P	0.64 kg
K_P	3.58 kN/m
V_{total}	349.6 cm^3
K_G	5.95 kN/m
$\dot{W}_{out}$	12.7 W per engine

Fig. 6 (*a*) Liquid rubber is cast in printed wax molds to fabricate the diaphragms. (*b*) Top wax mold and corrugated diaphragm after being separated from the molds.

gine system are tabulated in Table 1. Ambient pressure air was selected initially as the working fluid of the Stirling engines in order to avoid difficulties pertaining to gas containment during the laboratory tests. In order to eliminate surface-to-surface sliding friction, the pistons are realized by diaphragms, which also seal the engine chambers. Each piston is connected to the piston of its neighboring engine via a rigid linkage, and as will be explained, the motion of piston linkages is supported by a nylon cantilever flexure. Several subsystems constitute the fabricated prototype and will be discussed in the sequel.

5.1 Heat Exchangers. Heat exchangers have crucial roles in a Stirling engine system. A good heat exchanger design provides a balance between fluid flow friction and heat transfer characteristics. Heat exchangers with a wide frontal open area and short axial length together with an optimized hydraulic diameter are acceptable designs. Figure 5 shows the fabricated heat exchanger screens and the heater housing. The power resistors attached to the outside perimeter of the heater housing act as the heating source. The regenerator is a stack of woven-wire screens with circular cross-section wire, whereas the heater and cooler are stacks of etched copper screens (not woven) with square cross-section etched wire. Furthermore, in addition to its conventional sealing task, the o-ring is designed to act as a spacer between hot and cold sides of each engine to minimize the static heat loss from hot side of the engine to its cold side.

For flow friction, as discussed in Ref. [2], there are several approaches suggested in the literature. Estimated efficiencies based on the correlation of Tanaka et al. are reported in Ref. [10] to be higher than experimental measurements. Furthermore, since
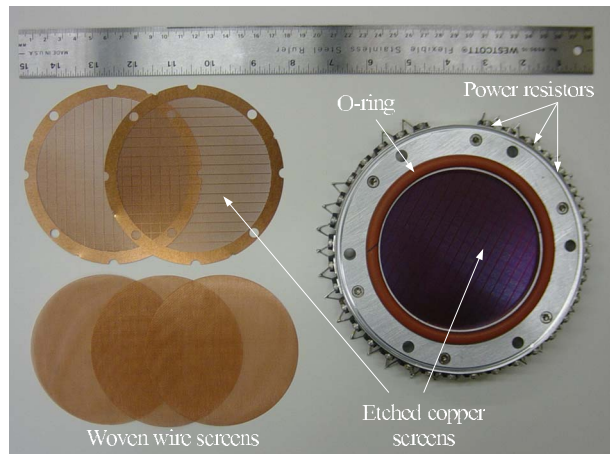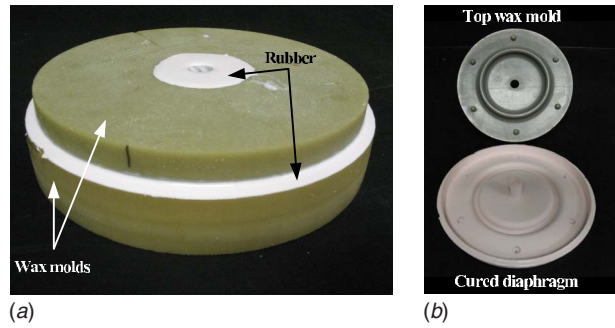
the working fluid conditions of the experiments of Tanaka et al. (e.g., temperature, pressure, fluid type, and Reynolds number) fit in the range of conditions for the engine discussed here, the correlation of Tanaka et al. was trusted in design computations.

5.2 Diaphragm Pistons. Mechanical friction is virtually eliminated by replacing moving pistons by diaphragms. Thus, losses associated with surface-to-surface sliding friction and lifetime limitations associated with mechanical wear are avoided. As a further consequence, lack of static friction enables the engine system to self-start upon application of heat, as discussed in Sec. 4. In addition, there is no issue with sealing requirements that have plagued Stirling designs with conventional crank mechanism.

The piston diameter (10 cm) and excursion (1 cm) were initially chosen based on the very simple Beale analysis [5] to produce 70 W output power per engine at 50 Hz operating frequency. However, later on, in order to avoid the nonlinear stiffness of a flat diaphragm, the piston diameter was reduced to 7.6 cm to accommodate a thicker diaphragm with one ring of corrugation. This change, of course, reduced the gas spring stiffness and set the operating frequency to about 30 Hz, based on the analysis in Sec. 4. This change reduced the indicated output power to 12.7 W, as shown in Table 1.

The corrugated diaphragms are fabricated by casting silicone rubber in custom-made wax molds, which are produced by a three-dimensional printer. Figure 6 illustrates the fabrication process and Fig. 7 shows the trimmed diaphragm that is attached to the system.

5.3 Flexure. A rigid arm, the piston linkage, connects the expansion piston plate of one engine to the compression piston plate of the other. For each piston linkage, a bearing function is
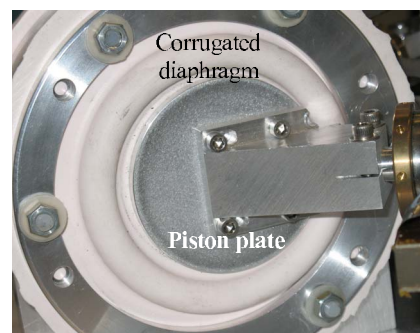

Fig. 5 Fabricated heat exchanger frame and the screens

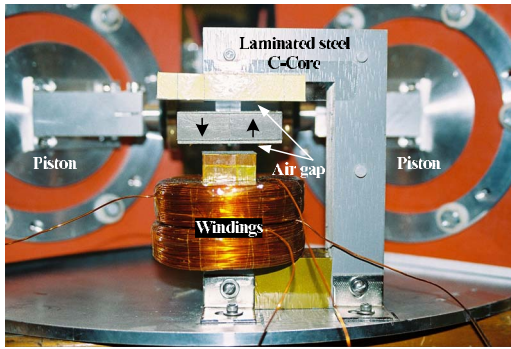**Fig. 7 Close-up view of the fabricated diaphragm with one ring of corrugation**

Fig. 8 Fabricated magnetic actuator (control circuitry not shown)

realized with a nylon cantilever flexure. This flexure has to be designed to be very stiff in the axial and radial directions, but with low loss and low stiffness for angular motion. Variation in the pressure inside each engine chamber translates into force on each piston plate, and a radial force component is applied to the flexure in this design. The maximum or critical radial force, F_r, that the flexure can withstand before buckling is given by,

$$F_r = \left(\frac{\pi}{2.1}\right)^2 EI \frac{1}{l^2} \qquad (27)$$

where E is the elasticity modulus of the flexure material, $I = \frac{1}{12} ht^3$ is the second moment of area, t is the flexure thickness, h is the flexure height in axial direction, and l is the flexure length in radial direction. The flexure dimensions should be chosen such that the flexure cross-sectional area is large enough to keep the radial stress well within the maximum tensile strength of the flexure material. Steel has a very high tensile strength limit. However, it is not an appropriate material choice due to its high elasticity modulus. In order to fulfill the low angular stiffness requirement, a thin sheet of steel would be required that, in turn, would not withstand the buckling force. Nylon with maximum tensile strength of about 60 MPa and elasticity modulus of about 1 GPa turns out to be a good choice of material for the three flexures.

The flexure dimensions are chosen as $t = 1.3$ mm, $l = 10$ mm, and $h = 100$ mm.

5.4 Actuator. One of the three fabricated magnetic actuators is shown in Fig. 8, and the fabricated prototype engine is shown in Fig. 9. Magnets are connected to the jaw that is indicted in Fig. 9 and move as the pistons oscillate. Therefore, as a generator or motion sensor, when the pistons (and hence magnets) move, an alternating magnetic flux links the coils that, in turn, induces voltage on the winding terminals. On the other hand, as an actuator, when alternating current flows through the windings, the resulting electromagnetic force pushes the magnet pair back and forth depending on the direction of the current flow.

If the alternators are used as actuators, the system can be driven in the heat pump regime [2]. In addition, each Stirling engine may be driven (as an alpha-type machine) in pure displacement or compression modes using only two of the magnetic circuits. The latter two driving modes are particularly useful while assessing the fluid flow and gas spring hysteresis losses, respectively [2].

6 Experimental Results

This section summarizes the experimental results obtained with the symmetric three-phase Stirling engine system.

6.1 Fluid Flow Friction. A ring-down test [2] turns out to be the most appropriate method to evaluate frictional losses. Table 2 tabulates resonant frequency, f_r, quality factor, Q, and damping factor, D, of the ring-down tests that were carried out for various cases to estimate the contribution of each component on the overall system behavior, and in particular, power dissipation. Based on a separate measurement, the nylon flexure stiffness is about 350 N/m and its equivalent moving mass is about 0.64 kg. This information enables the calculation of the dissipated power loss at a design excursion of 1 cm. These data are tabulated in column $\dot{W}_{loss}^{meas}$, and the estimated dissipation at the 29.4 Hz operating frequency is listed in column $\dot{W}_{loss}^{est}$.

The nylon flexure, the diaphragms, and the magnetic stiffness of the actuator are the three components that contribute to the overall stiffness of the mass-spring system with the actuator stiffness being dominant, which basically sets the frequency of the
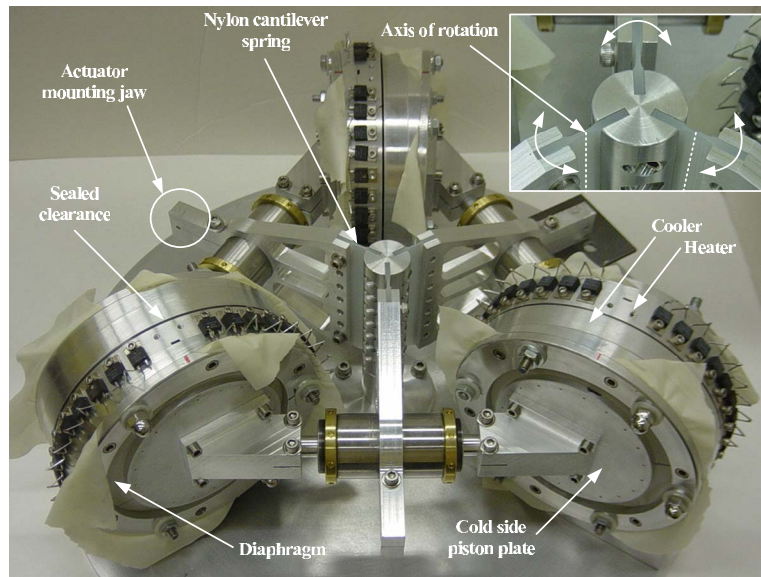

Fig. 9 Fabricated three-phase Stirling engine system. Photograph taken before custom corrugated silicone diaphragms were fabricated and installed.

Table 2   Summary of the ring-down tests carried out on the prototype. On each row the cross sign indicates which components were included in the test. F, D, K, H, R, and C refer to flexure, diaphragm, cooler, heater, regenerator, and C-core (actuator laminated steel core shown in Fig. 8), respectively.

F	D	K	H	R	C	f_r (Hz)	Q	D (N s/m)	$\overline{\dot{W}_{loss}^{meas}}$ at f_r (W)	$\overline{\dot{W}_{loss}^{est}}$ at 29.4 Hz (W)
×						3.7	26.7	0.56	0.02	0.96
×	×	×				7.5	10.8	2.78	0.31	4.74
×	×	×	×			7.5	8.9	3.42	0.38	5.84
×	×	×	×	×		7.5	6.3	4.80	0.53	8.19
×					×	10.2	65.4	0.62	0.13	1.06
×	×	×			×	11.9	19.3	2.49	0.70	4.25
×	×	×	×		×	11.9	17.4	2.76	0.77	4.71
×	×	×	×	×	×	11.9	9.5	5.07	1.42	8.65

displacement mode operation of the system to about 11.9 Hz.

We can infer the fluid flow loss contribution of the heater, cooler, and the regenerator at two frequencies (i.e., 7.5 Hz and 11.9 Hz) from Table 2. A comparison of the measured data for regenerator with the design values, Table 3, signifies that the flow friction correlations suggested by Tanaka et al. [10] for oscillating flow are reliable and even conservative. Hence, using such reliable correlations, one can be confident that the fabricated machine will not suffer from unexpected excessive flow friction.

6.2   Gas Spring Hysteresis. The calorimetric test [2] proved to be an appropriate method for the measurement of the gas hysteresis dissipation as well. A single engine phase is actuated at its pure compression resonant frequency (about 30 Hz) and, hence, the pistons are 180 deg out of phase with respect to each other. Under this condition, the working fluid is virtually not flowing through the heat exchangers. Therefore, the measured dissipation is solely related to the gas spring hysteresis. In order to observe the effect of the heat exchanger on gas spring hysteresis, four different conditions have been considered, as tabulated in Table 4. An estimation algorithm [2] is then utilized to estimate the amount of the generated heat (i.e., the loss within that component). In each case, a slightly different resonant frequency was observed for the compression mode that is due to the different volume of gas that is enclosed by the engine chamber. As one may expect, the measured data confirm that by decreasing the working gas volume (adding more screens inside the engine), the gas spring stiffness

increases that, in turn, increases the resonant frequency.

In Table 4, the measured gas spring hysteresis loss has been compared with the suggested formulation in Ref. [2]. This result confirms the accuracy of the calculation and provides a reliable basis for estimation of the compression losses that play a crucial role in the operation of free-piston Stirling engines. The measured data points are plotted in Fig. 10 versus fractional volumetric variation, and a quadratic curve fit through these data validates the theoretical modeling of the gas spring hysteresis dissipation discussed in Ref. [2].

6.3   Engine Operation. The gas spring hysteresis dissipation was not initially considered in the design, and it turns out that it is an important dissipation phenomenon and should be carefully addressed in the low-power Stirling engine design, as it hindered the operation of the test system in engine mode. At steady state, the phase delay between the two pistons of each Stirling engine is intended to be 120 deg. This condition translates into a fractional volumetric variation of about 0.4 for the working fluid inside the engine chamber. Hence, as shown in Fig. 10, the gas spring hysteresis loss would be about 10.8 W. This figure corresponds to a damping factor of about 6.1 N s/m. From a power balance point of view, the total losses in the system (i.e., viscous friction and gas spring hysteresis dissipation) are about 19.5 W per engine, which actually surpass the nominal output power of 12.7 W. On the other hand, with a total damping factor of 11.2 N s/m, according to Eq. (26), the start-up temperature is about 175°C. A direct numerical

Table 3   Comparison of the measured flow friction data with designed values for heater and regenerator

f (Hz)	$\overline{\dot{W}_{H,loss}^{calc}}$ (W)	$\overline{\dot{W}_{H,loss}^{meas}}$ (W)	$\overline{\dot{W}_{R,loss}^{calc}}$ (W)	$\overline{\dot{W}_{R,loss}^{meas}}$ (W)
7.5	0.04	0.07	0.65	0.15
11.9	0.13	0.07	1.7	0.65
29.4	1.2	0.46–1.1	7	2.35–3.94

Table 4   Comparison of measured and calculated gas spring hysteresis (compression) losses in various conditions. The number in the three leftmost columns indicate the fraction of corresponding heat exchanger screens that is in place.

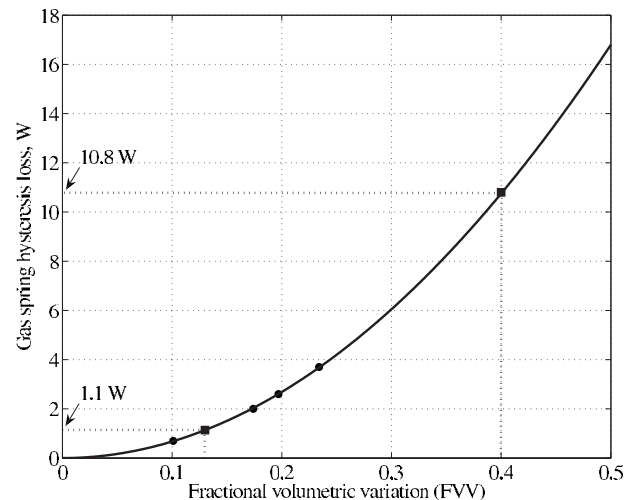| Heater (%)	Cooler (%)	Regen. (%)	f (Hz)	Piston stroke (mm)	$\dot{W}_{hys}^{calc}$ (W)	$\dot{W}_{hys}^{meas}$ (W)
0	0	0	28.2	12	2.3	2
50	50	0	29.2	12	2.6	2.6
100	100	0	29.6	13	3.7	3.7
50	50	50	30	6	0.7	0.7

Fig. 10   Gas spring hysteresis loss versus fractional volumetric variation. The graph is a quadratic regression through the measured points (shown in dots) taken from Table 4.

calculation of the eigenvalues of the linearized system [2] confirms the accuracy of the derived expression in Eq. (26). In addition to being significantly higher than the design temperature, the required start-up temperature surpasses the operating temperature limit of the rubber diaphragm (diaphragm material releases toxic gases at temperatures above 150°C). The computed start-up temperature is about 87°C considering the viscous dissipation only.

In order to decrease the gas spring hysteresis dissipation, as described in Ref. [2], reduction in fractional volumetric variation is the most effective strategy. If the fabricated engines (six of them) are assembled together in a six-phase system, the fundamental mode will result in a 60 deg phase delay between the pistons of each engine. This will reduce the fractional volumetric variation to 0.13, which reduces the gas spring hysteresis losses by an order of magnitude to 1.1 W, according to Fig. 10. In addition, the operating frequency drops to about 19.4 Hz, which further decreases the gas spring hysteresis dissipation to 0.9 W and the viscous losses to 3.7 W. Therefore, the total damping factor is 6.3 N s/m, which corresponds to a start-up temperature of about 79°C (refer to Ref. [2] for details). From the power balance point of view, the indicated output power in this case is about 10 W with a total dissipation of 4.6 W. These figures confirm the possibility of operation in engine mode.

Therefore, attempting a six-phase system is very interesting and promising. However, it is even more interesting if the kinematics of a symmetric three-phase system is slightly modified to force the pistons of each engine to oscillate with a 60 deg phase delay instead of the classical 120 deg. Such a system will have half of the parts (moving or not) that otherwise would be required for a successful operation. The following section introduces what is called a reverser in this paper and provides the required theoretic background for dynamical analysis of a multiphase Stirling engine that utilizes a reverser.

7 Reverser Modeling and Analysis

For the fundamental mode of an N-phase system ($N > 3$) with an even number of phases, there are $N/2$ pairs of pistons with equal and opposite trajectories. In such cases, by utilizing a reversing mechanism for one of the piston linkages, half of the engine chambers can be eliminated without altering the phase relationship among the remaining pistons. In a conventional multiphase system, as explained before, the expansion piston of each Stirling engine is rigidly connected to the compression piston of its neighboring engine. Therefore, if the expansion piston of the ith engine moves in, the compression piston of the $(i+1)$th engine will move out. However, if those two pistons are connected via a
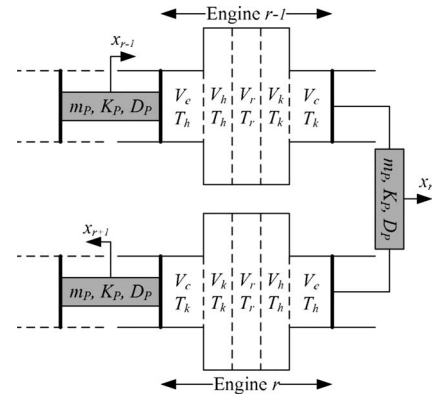

Fig. 11 Schematic of a multiphase Stirling engine system that incorporates a reversing mechanism within piston *r*

reverser, the inward motion of the expansion piston of the ith engine will force the compression piston of the $(i+1)$th engine to move in as well.

Figure 11 shows the schematic of a multiphase Stirling engine system with the rth piston acting as a reverser. Newton's second law for the reversing piston is expressed as Eq. (28), which can be substituted into Eq. (5) to define the nonlinear dynamical behavior of a multiphase Stirling engine system that is equipped with a reverser

$$A_P(p_{r-1} + p_r - 2p_o) - f_P(\dot{x}_r) - K_P x_r = m_P \ddot{x}_r \qquad (28)$$

where p_o is the ambient or bounce space pressure. It should be noted that, due to the reversing mechanism of piston r, we have

$$V_{e,r} = V_e^{\text{nom}} + A_P x_r \qquad (29)$$

However, for all other expansion and compression volumes, Eqs. (3) and (4) are still valid.

Therefore, in a system where the rth piston is a reverser, Eq. (6) should be replaced by Eq. (30) for the rth piston and by Eq. (31) for the $(r+1)$th piston, respectively

$$\ddot{x}_r = \left(\frac{\alpha}{m_P}\frac{1}{T_h}\right)x_{r-1} - \left(\frac{\alpha}{m_P}\frac{1}{T_h} + \frac{\alpha}{m_P}\frac{1}{T_k} + \frac{K_P}{m_P}\right)x_r - \left(\frac{\alpha}{m_P}\frac{1}{T_k}\right)x_{r+1} - d\dot{x}_r$$
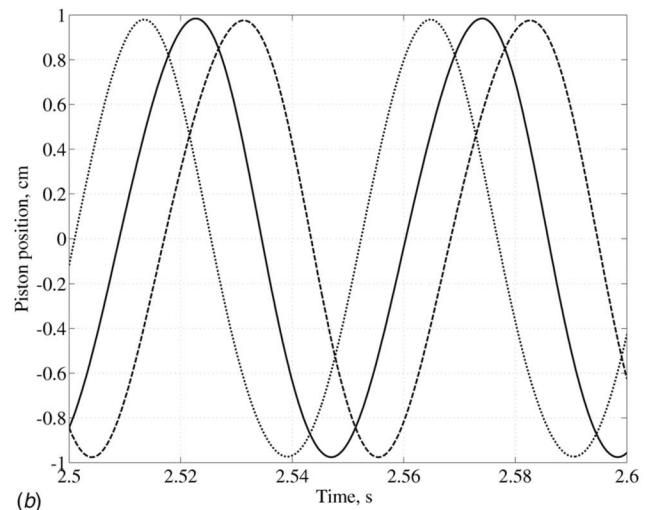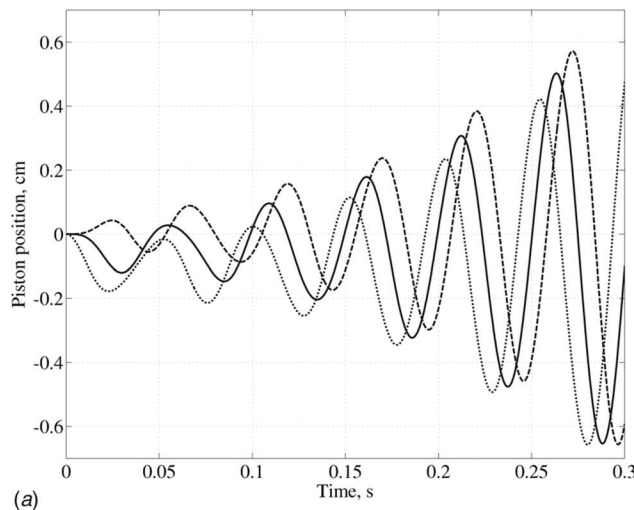
$$(30)$$

Fig. 12 Simulated piston positions of the three-phase system with reverser: (*a*) startup and (*b*) steady state
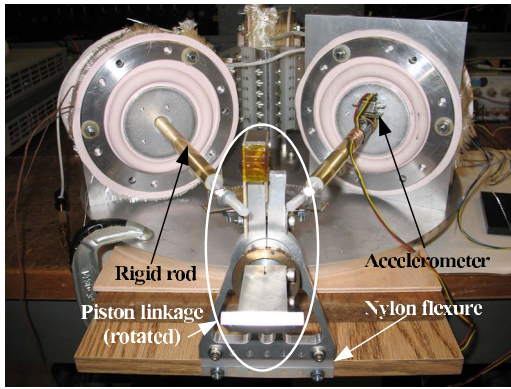
Fig. 13 Implementation of reverser mechanism within the fabricated three-phase Stirling engine prototype

(a)

(b)

(c)

Fig. 14 Recorded acceleration signals of the three phases in the revised three-phase Stirling engine system

$$\ddot{x}_{r+1} = -\left(\frac{\alpha}{m_P}\frac{1}{T_h}\right)x_r - \left(\frac{\alpha}{m_P}\frac{1}{T_h} + \frac{\alpha}{m_P}\frac{1}{T_k} + \frac{K_P}{m_P}\right)x_{r+1} + \left(\frac{\alpha}{m_P}\frac{1}{T_k}\right)x_{r+2}$$
$$- d\dot{x}_{r+1} \tag{31}$$

Hence, the linearized dynamics of an N-phase Stirling engine system with piston $r < N$ as the reverser can still be represented by Eq. (8), if the element $(r, r+1)$ of the stiffness matrix is replaced with $+b$ and the element $(r+1, r)$ is replaced with $+c$.

If the second linkage of a symmetric three-phase Stirling system is replaced with a reverser (i.e., $r=2$), matrix **K** in Eq. (12) becomes

$$\mathbf{K} = \begin{bmatrix} \frac{K_P}{m_P} + (b+c) & -b & -c \\ -c & \frac{K_P}{m_P} + (b+c) & +b \\ -b & +c & \frac{K_P}{m_P} + (b+c) \end{bmatrix} \tag{32}$$

By applying the transformation $\mathbf{x} = \mathbf{Tz}$ with

$$\mathbf{T} = \begin{bmatrix} -1 & 0 & 1 \\ 1 & \sqrt{3}/2 & 1/2 \\ 1 & -\sqrt{3}/2 & 1/2 \end{bmatrix} \tag{33}$$

the state-space representation of the system becomes

$$\begin{bmatrix} \ddot{z}_1 \\ \ddot{z}_2 \\ \ddot{z}_3 \end{bmatrix} + d\begin{bmatrix} \dot{z}_1 \\ \dot{z}_2 \\ \dot{z}_3 \end{bmatrix} + \begin{bmatrix} \frac{K_P}{m_P} + 2(b+c) & 0 & 0 \\ 0 & \frac{K_P}{m_P} + \frac{1}{2}(b+c) & -\frac{\sqrt{3}}{2}(b-c) \\ 0 & \frac{\sqrt{3}}{2}(b-c) & \frac{K_P}{m_P} + \frac{1}{2}(b+c) \end{bmatrix}$$
$$\times \begin{bmatrix} z_1 \\ z_2 \\ z_3 \end{bmatrix} = 0 \tag{34}$$

which simply reveals the following three eigenvalues for the stiffness matrix:
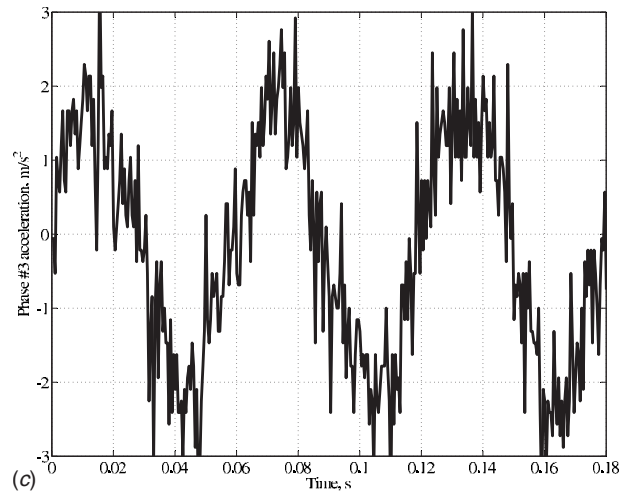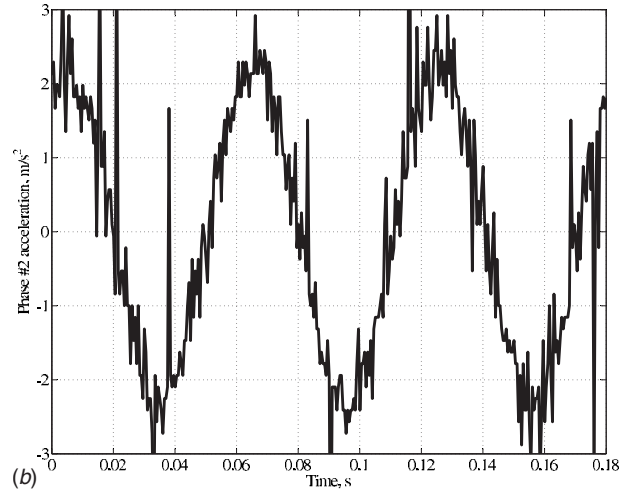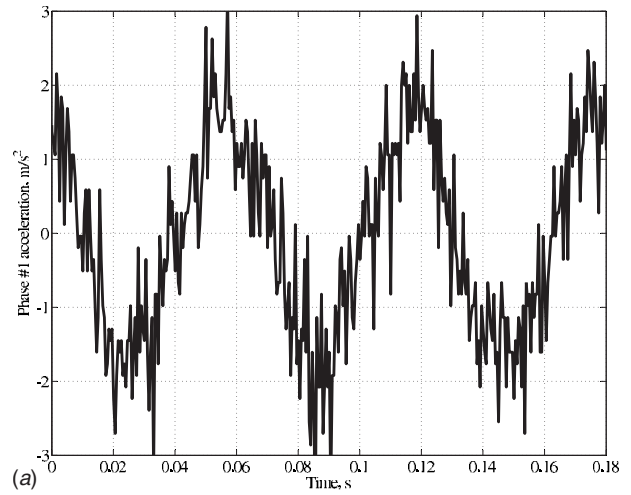
$$\mu_1 = \frac{K_P}{m_P} + 2(b+c) \tag{35}$$

$$\mu_{2,3} = \left(\frac{K_P}{m_P} + \frac{1}{2}(b+c)\right) \pm J\frac{\sqrt{3}}{2}(b-c) \tag{36}$$

It is very interesting to note that none of the modes associated with the three-phase system are present here. However, the modes are identical to a subset of the modes of a six-phase system that are discussed in Ref. [2]. Based on that discussion, μ_1 represents the "pure compression" mode. The remaining two eigenvalues
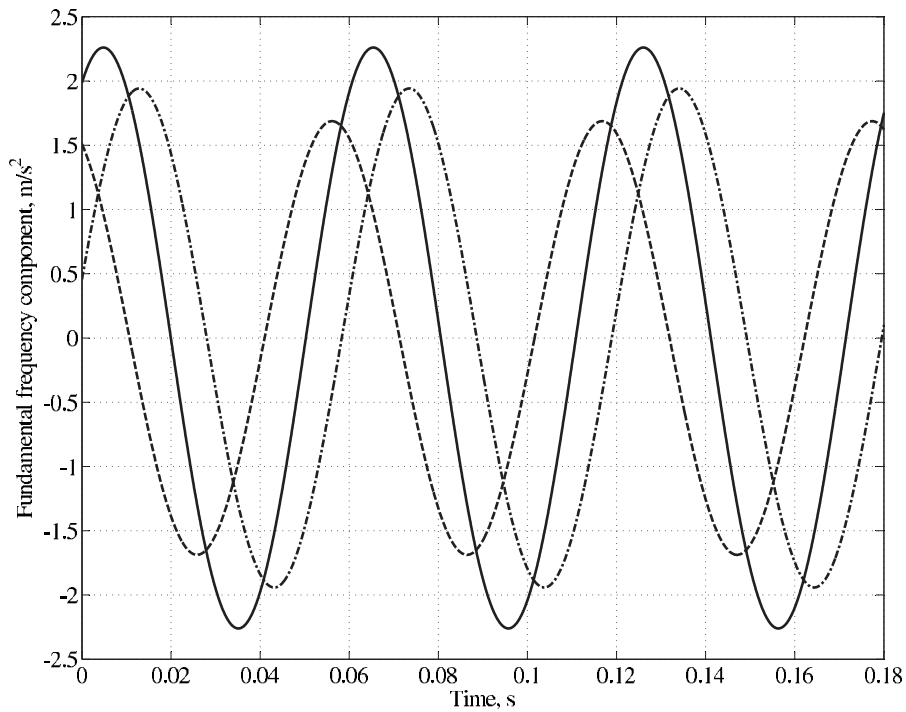
Fig. 15 Fundamental frequency components of the three acceleration signals. Compare to Fig. 12(b).

correspond to the fundamental forward and backward six-phase operation of the system. This guarantees a 60 deg phase delay between the pistons of each engine in a three-phase system that utilizes a reverser.

Following a similar approach to the symmetric three-phase case, the relationship between the damping factor and start-up temperature becomes

$$\frac{1}{T_h} = \frac{1}{T_k} - \frac{d}{\alpha}\sqrt{\frac{4}{3}m_P(K_P + K_G)} \qquad (37)$$

which indicates that both the resonant frequency and start-up temperature of this system will be lower than its symmetric three-phase counterpart. Based on this analysis, an operating resonant
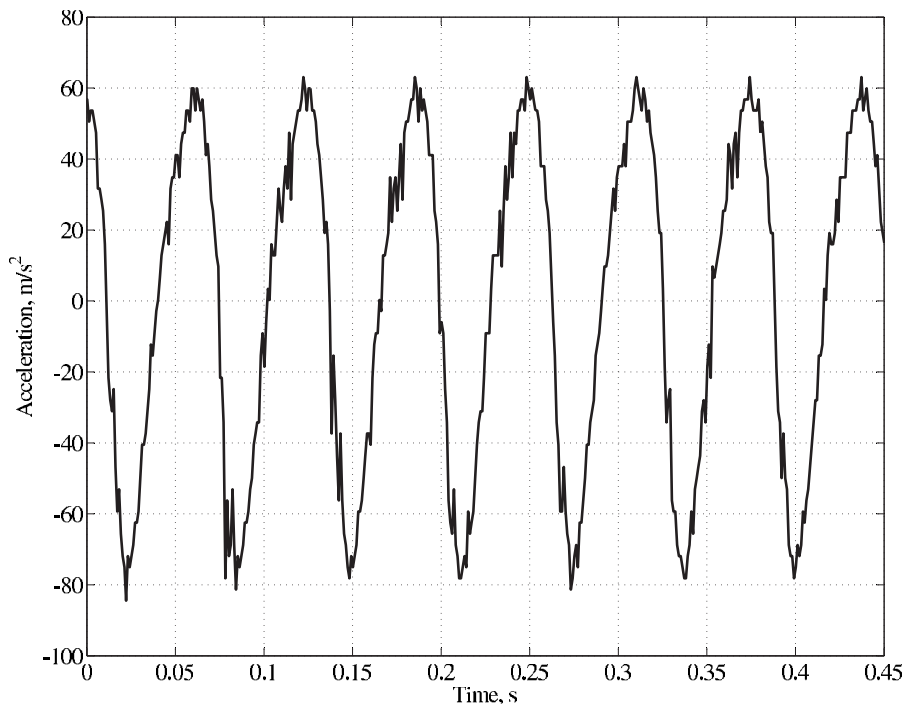

Fig. 16 Acceleration signal of one piston at full-amplitude oscillation

frequency of 19 Hz and a start-up temperature of 79°C are estimated for the revised system. The simulation result of the same system is depicted in Fig. 12.

8 Reverser Implementation

Figure 13 illustrates the implementation of a reverser system within the fabricated prototype. The rigid rods are very light tubes to help the system retain its symmetry (i.e., equal mass and external stiffness for all three engines). All three heaters of the system are heated by electric heating elements that is wrapped on their outer perimeter. As the expansion space temperature increases, the system exhibits higher quality factor if examined by a ring-down test. As soon as the temperature reaches about 100°C, the engine starts. Note that the cold side temperature is about 40°C. In this condition, the computed start-up temperature is 94°C.

Figure 14 depicts the recorded acceleration signals of the three phases at small excursions. The extracted fundamental frequency components of the acceleration signals are shown in Fig. 15. The signals show an oscillation frequency of about 16 Hz and 60 deg phase delays between the three phases, as expected. At large excursions, the pistons oscillate at magnitudes of about 0.7 cm according to Fig. 16.

9 Conclusions

Mathematical modeling of multiphase Stirling engine systems was presented in this paper. A symmetric three-phase system was discussed in detail based on modal analysis of the corresponding linearization. This analysis proved the self-starting potential of multiphase systems. The start-up temperature of the heater, at which the system started its operation, was derived based on the same modal analysis. The operation of a low-temperature three-phase Stirling engine prototype in engine mode was discussed based on the developed modal analysis and internal gas spring hysteresis dissipation of the engines.

Design, fabrication, and test of a symmetric three-phase free-piston Stirling engine system were discussed as well. Diaphragm pistons and nylon flexures are considered for this prototype to eliminate surface friction and to provide appropriate seals. The experimental results were presented and compared with design calculations. Tests confirmed the design models for heat exchanger flow friction losses and gas spring hysteresis dissipation. However, it was revealed that gas spring hysteresis loss was an important dissipation phenomenon for low-power systems, and should be carefully addressed in design as it hindered the operation of the symmetric three-phase prototype.

Further analysis showed that the gas hysteresis dissipation was reduced drastically by increasing the number of phases in a system with a little compromise on the operating frequency and, hence, the output power. It was further shown that for an even number of phases, half of the pistons could be eliminated by utilizing a reverser. The mathematical formulation and modal analysis of multiphase Stirling engine system was then extended to incorporate a reverser. By introducing a reverser to the fabricated prototype, the system proved its self-starting capability in engine mode and validated the derived expression for computing the start-up temperature.

References

[1] Der Minassians, A., Aschenbach, K. H., and Sanders, S. R., 2004, "Low-Cost Distributed Solar-Thermal-Electric Power Generation," Proc. SPIE, **5185**, pp. 89–98.

[2] Der Minassians, A., 2007, "Stirling Engines for Low-Temperature Solar-Thermal-Electric Power Generation," Ph.D. thesis, EECS Department, University of California, Berkeley, Berkeley, http://www.eecs.berkeley.edu/Pubs/TechRpts/2007/EECS-2007-172.html.

[3] Welford, W. T., and Winston, R., 1989, *High Collection Nonimaging Optics*, Academic, San Diego, CA.

[4] Senft, J. R., 2002, *An Introduction to Low Temperature Differential Stirling Engines*, 5th ed., Moriya, River Falls, WI.

[5] Urieli, I., and Berchowitz, D. M., 1984, *Stirling Cycle Engine Analysis*, Adam Hilger, Bristol.

[6] Der Minassians, A., and Sanders, S. R., 2007, "A Magnetically-Actuated Resonant-Displacer Free-Piston Stirling Machine," Fifth International Energy Conversion Engineering Conference, IECEC.

[7] Sastry, S., 1999, *Nonlinear Systems: Analysis, Stability, and Control*, 1st ed., Springer, New York.

[8] Krause, P. C., Sudhoff, S. D., and Wasynczuk, O., 1995, *Analysis of Electric Machinery*, IEEE, New York.

[9] Der Minassians, A., and Sanders, S. R., 2007, "Multiphase Free-Piston Stirling Engine for Solar-Thermal-Electric Power Generation Applications," 5th International Energy Conversion Engineering Conference.

[10] Tanaka, M., Yamashita, I., and Chisaka, F., 1990, "Flow and Heat Transfer Characteristics of the Stirling Engine Regenerator in an Oscillating Flow," JSME Int. J., Ser. II, **33**, pp. 283–289.